COMPUTER METHODS IN MATERIALS SCIENCE

2022, vol. 22, no. 1, 13–22
https://doi.org/10.7494/cmms.2022.1.0771

Modeling of temperature-dependent cyclic performance of superelastic NiTi shape memory alloy

Yao Xiao[1,2*], Shuangyan Ju[1], Jianping Lin[1]

[1] School of Mechanical Engineering, Tongji University, 201804 Shanghai, China.
[2] Institute for Advanced Study, Tongji University, 200092 Shanghai, China.

Abstract

In this paper, a three-dimensional micromechanical-based constitutive model is proposed to describe the temperature-dependent performance of a cyclic deformed superelastic NiTi shape memory alloy. The dominant texture of the specimen is prescribed as <111> direction along the longitudinal direction. Apart from martensitic transformation, various mechanisms regarding superelastic degradation are taken into consideration. In order to be extended from the single-crystal scale to the polycrystalline version, the constitutive model is implemented into finite element software. It is verified that the measured cyclic response of a superelastic NiTi is well reproduced by the presented approach. Furthermore, the predicting capability of the proposed model is verified by simulating the mechanical behavior of NiTi tube subjected to cyclic bending.

Keywords: shape memory alloy, phase transformation, micromechanics

1. Introduction

The NiTi shape memory alloy (SMA) is one of the most successful SMAs in aeronautics, energy conversion, energy storage, and automotive applications due to its superior mechanical properties (Otsuka & Ren, 2005; Šittner et al., 2018). The growing demand for using NiTi SMAs in industry is pushing researchers to develop effective and efficient simulation tools. To this end, numerous constitutive models have been applied to study the mechanical behavior of NiTi (Cisse et al., 2016). These models can mainly be classified into two categories, i.e. macro phenomenological model and micromechanical-based one. Generally, the phenomenological model tracks the total martensite volume fraction instead of the individual martensite variant. Its key advantages lie in higher computational efficiency, easier parameter calibration and more convenient implementation into finite element software. Nevertheless, since the microstructure (i.e. grain size, texture, etc.) plays an important role in the mechanical performance of NiTi, micromechanical modelling is a promising fashion to provide in-depth insights into the underlying deformation mechanisms. The major challenge of the micromechanical-based model is that it is constructed based on the behavior of a single crystal (or a single representative volume element), and its applicability in modeling the response of a polycrystalline NiTi remains a key issue.

Superelastic NiTis exhibit superelasticity degeneration during cyclic deformation (Kang et al., 2009; Wagner et al., 2004; Xiao & Jiang, 2020). Recently, a few micromechanical-based models have been established to describe the plastic deformation of NiTi (Dhala et al., 2019; Manchiraju & Anderson, 2010; Sadjadpour & Bhattacharya, 2007; Wang et al., 2008; Yan et al., 2021; Yu et al., 2014a, 2014b, 2015, 2017). Via the introduction of the

*Corresponding author: xiaoy10@tongji.edu.cn
ORCID ID's: 0000-0003-3011-8408 (Y. Xiao), 0000-0002-9538-1066 (S. Ju), 0000-0002-1355-3638 (J. Lin)

effective transformation strain of martensite, Sadjadpour & Bhattacharya (2007) proposed a micromechanics-inspired constitutive model incorporating transformation as well as plastic strain. Wang et al. (2008) built a micromechanical constitutive model for superelastic NiTis. The model reasonably predicted the multiaxial behavior and tension-compression asymmetry of a NiTi by introducing both deformation twinning and dislocation slip. Manchiraju & Anderson (2010) constructed a crystal plasticity approach coupling transformation and plasticity via stress redistribution. Single crystal behavior, superelastic response of randomly oriented polycrystalline, and the stress-biased two-way shape memory effect were replicated. Yu et al. (2014a, 2014b, 2015, 2017) proposed several constitutive models based on crystal plasticity to simulate the deformation and superelasticity degeneration of a NiTi by incorporating various inelastic mechanisms. For the sake of simplicity, an explicit scale transition rule was utilized to obtain the polycrystalline response from tens to hundreds of single crystals.

In this paper, a micromechanical-based constitutive model was constructed and implemented into finite element software. As an advance of the previous studies (Xiao et al., 2018; Yu et al., 2014a, 2014b, 2015, 2017), the effects of temperature on the elastic deformation, martensitic transformation and superelastic degradation of a cyclically deformed NiTi are considered. The simulation results are in general agreement with the experiments. Cyclic bending performance is also emulated to demonstrate the model's prediction capability. The paper is organized as follows. In section 2, a micromechanical-based constitutive model is proposed. Verification of the model and discussion on simulation results are provided in section 3. Conclusions are drawn in section 4.

2. Constitutive Model

2.1. Definition of strain

Based on the hypothesis of small deformation, the total strain $\boldsymbol{\varepsilon}$ is decomposed into the elastic strain $\boldsymbol{\varepsilon}^{e}$, the transformation strain $\boldsymbol{\varepsilon}^{tr}$, and the transformation-induced plastic strain $\boldsymbol{\varepsilon}^{tp}$:

$$\varepsilon = \varepsilon^{e} + \varepsilon^{tr} + \varepsilon^{tp} \tag{1}$$

In the present work, primary attention is paid to a superelastic NiTi and stress-induced martensitic transformation, so martensite detwinning is not taken into account. The transformation strain can therefore be attributed to <011> Type II twinning with 24 habit plane variants (Gall et al., 2000; Long et al., 2017, 2020; Otsuka & Ren, 2005; Thamburaja & Anand, 2003; Xiao et al., 2018). The local orientation tensor of the α-th martensite variant $\mathbf{L}^{\alpha}$ in the crystal coordinate is given by:

$$\mathbf{L}^{\alpha} = \frac{1}{2}\left(\mathbf{m}^{\alpha} \otimes \mathbf{n}^{\alpha} + \mathbf{n}^{\alpha} \otimes \mathbf{m}^{\alpha}\right) \tag{2}$$

where $\mathbf{m}^{\alpha}$ and $\mathbf{n}^{\alpha}$ are the transformation direction and the habit plane normal of the α-th martensite variant, respectively. The values of $\mathbf{m}^{\alpha}$ and $\mathbf{n}^{\alpha}$ are listed in Table 1 (Wang et al., 2008) $\mathbf{L}^{\alpha}$ is defined in the crystal coordinate, and it should be transformed into the global coordinate for further analysis:

$$\mathbf{P}^{\alpha} = \mathbf{R}^{T}\mathbf{L}^{\alpha}\mathbf{R} \tag{3}$$

where $\mathbf{R}$ is the transformation matrix of the grain, and $\mathbf{R}^{T}$ is the transpose of $\mathbf{R}$. The transformation strain is written as:

$$\boldsymbol{\varepsilon}^{tr} = \sum_{\alpha=1}^{24} \xi^{\alpha} g^{tr} \mathbf{P}^{\alpha} \tag{4}$$

where g^{tr} is the magnitude of the transformation strain, and ξ^{α} is the volume fraction of the α-th martensite variant. Naturally, the total volume fraction of martensite is formulated as:

$$\xi = \sum_{\alpha=1}^{24} \xi^{\alpha} \tag{5}$$

Table 1. Transformation systems of NiTi
$(m_1, m_2, m_3) = (0.4114, -0.4981, 0.7633)$,
$(n_1, n_2, n_3) = (-0.8889, -0.4044, 0.2152)$ (Wang et al., 2008)

α	$\mathbf{m}^{\alpha}$			$\mathbf{n}^{\alpha}$		
1	n_1	n_2	n_3	n_1	n_2	n_3
2	n_2	n_1	$-n_3$	n_2	n_1	$-n_3$
3	$-n_1$	$-n_2$	n_3	$-n_1$	$-n_2$	n_3
4	$-n_2$	$-n_1$	$-n_3$	$-n_2$	$-n_1$	$-n_3$
5	n_1	$-n_2$	$-n_3$	n_1	$-n_2$	$-n_3$
6	$-n_2$	n_1	n_3	$-n_2$	n_1	n_3
7	$-n_1$	n_2	$-n_3$	$-n_1$	n_2	$-n_3$
8	n_2	$-n_1$	n_3	n_2	$-n_1$	n_3
9	n_3	$-n_1$	$-n_2$	n_3	$-n_1$	$-n_2$
10	n_3	n_1	n_2	n_3	n_1	n_2
11	$-n_3$	n_2	n_1	$-n_3$	n_2	n_1
12	$-n_3$	$-n_2$	$-n_1$	$-n_3$	$-n_2$	$-n_1$
13	$-n_3$	$-n_1$	n_2	$-n_3$	$-n_1$	n_2
14	$-n_3$	n_1	$-n_2$	$-n_3$	n_1	$-n_2$
15	n_3	$-n_2$	n_1	n_3	$-n_2$	n_1
16	n_3	n_2	$-n_1$	n_3	n_2	$-n_1$
17	$-n_1$	$-n_3$	$-n_2$	$-n_1$	$-n_3$	$-n_2$
18	n_1	$-n_3$	n_2	n_1	$-n_3$	n_2
19	$-n_2$	n_3	$-n_1$	$-n_2$	n_3	$-n_1$
20	n_2	n_3	n_1	n_2	n_3	n_1
21	$-n_1$	n_3	n_2	$-n_1$	n_3	n_2
22	n_1	n_3	$-n_2$	n_1	n_3	$-n_2$
23	n_2	$-n_3$	$-n_1$	n_2	$-n_3$	$-n_1$
24	$-n_2$	$-n_3$	n_1	$-n_2$	$-n_3$	n_1

As commented by Yu et al. (2015, 2017), the slipping direction of the interface between austenite and the α-th martensite variant can be assumed to be identical to that of the α-th transformation system. So $\boldsymbol{\varepsilon}^{tp}$ can be written as:

$$\boldsymbol{\varepsilon}^{tp} = \sum_{\alpha=1}^{24} \gamma_{tp}^{\alpha} \mathbf{P}^{\alpha} \tag{6}$$

where γ_{tp}^{α} is the slipping magnitude of the α-th equivalent slipping system, which increases gradually as martensitic transformation proceeds.

2.2. Framework of thermodynamics

Helmholtz free energy of the NiTi is decomposed into five portions:

$$\phi = \phi^{e} + \phi^{ch} + \phi^{h} + \phi^{tp} + \phi^{int} \tag{7}$$

where ϕ^{e} is the elastic energy, ϕ^{ch} is the chemical energy, ϕ^{h} is the hardening energy caused by martensitic transformation, ϕ^{tp} is the energy related to transformation-induced plasticity, and ϕ^{int} is the energy related to the accumulation of internal stress. ϕ^{e} is written as:

$$\phi^{e} = \frac{1}{2}\boldsymbol{\varepsilon}^{e} : \mathbf{C} : \boldsymbol{\varepsilon}^{e} \tag{8}$$

where $\mathbf{C}$ is the effective elastic tensor, $\mathbf{C} = \xi\mathbf{C}_{\mathrm{A}} + (1-\xi)\mathbf{C}_{\mathrm{M}}$. $\mathbf{C}_{\mathrm{A}}$ and $\mathbf{C}_{\mathrm{M}}$ are the elastic tensors of austenite and martensite, respectively. ϕ^{ch} is expressed as:

$$\phi^{ch} = c\left[\left(T - T_0\right) - T\ln\left(\frac{T}{T_0}\right)\right] + \nu\left(T - T_0\right)\xi \tag{9}$$

where c is the specific heat capacity, T_0 is the balance temperature, and v is the material constant reflecting the temperature dependence of martensitic transformation (Churchill et al., 2009; Liu et al., 2008; Xiao et al., 2017). The rate evolution of ϕ^{h} is given as:

$$\dot{\phi}^{h} = \sum_{\alpha=1}^{24} X^{\alpha}\dot{\xi}^{\alpha} \tag{10}$$

$$X^{\alpha} = H^{\alpha}\xi^{\alpha} \tag{11}$$

where X^{α} and H^{α} are the hardening resistance and the hardening modulus of the α-th martensite variant, respectively. Similarly, the rate evolution of ϕ^{tp} is expressed as:

$$\dot{\phi}^{tp} = \sum_{\alpha=1}^{24} \tau_{tp}^{\alpha}\left|\dot{\gamma}_{tp}^{\alpha}\right| \tag{12}$$

where τ_{tp}^{α} is the slipping resistance of the α-th equivalent slipping system and is written as:

$$\tau_{tp}^{\alpha} = H_{tp}\bar{\gamma}_{tp}^{\alpha} \tag{13}$$

where $\bar{\gamma}_{tp}^{\alpha}$ is the accumulated slipping of the α-th martensite variant and is defined as:

$$\dot{\bar{\gamma}}_{tp}^{\alpha} = \left|\dot{\gamma}_{tp}^{\alpha}\right| \tag{14}$$

The evolution law of ϕ^{int} yields:

$$\dot{\phi}^{\mathrm{int}} = -\mathbf{B}_{tr} : \dot{\varepsilon}^{tr} \tag{15}$$

$$\mathbf{B}_{tr} = \sum_{\alpha=1}^{24} B_{tr}^{\alpha}\mathbf{P}^{\alpha} \tag{16}$$

The reduced Clausius–Duhem inequality is formulated as:

$$\Gamma = \boldsymbol{\sigma} : \dot{\varepsilon} - \dot{\phi} - \kappa\dot{T} \geq 0 \tag{17}$$

where κ is the specific entropy. Substituting Equations (4) to (16) into (17), one can derive:

$$\begin{aligned}\Gamma = &\left(\boldsymbol{\sigma} - \frac{\partial\phi}{\partial\boldsymbol{\varepsilon}^{e}}\right) : \dot{\varepsilon} - \left(\kappa + \frac{\partial\phi}{\partial T}\right)\dot{T} + \\ &\sum_{\alpha=1}^{24}\left[g^{tr}\left(\boldsymbol{\sigma} + \mathbf{B}_{tr}\right) : \mathbf{P}^{\alpha} - \upsilon\left(T - T_0\right) - \right. \\ &\left. H^{\alpha}\xi^{\alpha} - \frac{1}{2}\boldsymbol{\varepsilon}^{e} : \left(\mathbf{C}_{M} - \mathbf{C}_{A}\right) : \boldsymbol{\varepsilon}^{e}\right]\dot{\xi}^{\alpha} + \\ &\sum_{\alpha=1}^{24}\left(\boldsymbol{\sigma} : \mathbf{P}^{\alpha}\dot{\gamma}_{tp}^{\alpha} - H_{tp}\bar{\gamma}_{tp}^{\alpha}\left|\dot{\gamma}_{tp}^{\alpha}\right|\right) \geq 0\end{aligned} \tag{18}$$

Equation (18) is positive regardless of the thermomechanical loading paths. It is reasonable to presume that:

$$\mathrm{sign}(\boldsymbol{\sigma} : \mathbf{P}^{\alpha}) = \mathrm{sign}(\dot{\gamma}_{tp}^{\alpha}) \tag{19}$$

where

$$\mathrm{sign}(x) = \begin{cases} 1 & \text{if } x > 0 \\ -1 & \text{if } x < 0 \\ 0 & \text{if } x = 0 \end{cases} \tag{20}$$

With Equations (19) and (20), Equation (18) is rewritten as:

$$\begin{aligned}\Gamma = &\left(\boldsymbol{\sigma} - \frac{\partial\phi}{\partial\boldsymbol{\varepsilon}^{e}}\right) : \dot{\varepsilon} - \left(\kappa + \frac{\partial\phi}{\partial T}\right)\dot{T} + \\ &\sum_{\alpha=1}^{24}\left[g^{tr}\left(\boldsymbol{\sigma} + \mathbf{B}_{tr}\right) : P^{\alpha} - \upsilon\left(T - T_0\right) - \right. \\ &\left. H^{\alpha}\xi^{\alpha} - \frac{1}{2}\boldsymbol{\varepsilon}^{e} : \left(\mathbf{C}_{M} - \mathbf{C}_{A}\right) : \boldsymbol{\varepsilon}^{e}\right]\dot{\xi}^{\alpha} + \\ &\sum_{\alpha=1}^{24}\left(\left|\boldsymbol{\sigma} : \mathbf{P}^{\alpha}\right| - H_{tp}\bar{\gamma}_{tp}^{\alpha}\right)\left|\dot{\gamma}_{tp}^{\alpha}\right| \geq 0\end{aligned} \tag{21}$$

Basically, the stress and the entropy take the following forms:

$$\boldsymbol{\sigma} = \frac{\partial \phi}{\partial \boldsymbol{\varepsilon}^e} = \mathbf{C} : \left(\boldsymbol{\varepsilon} - \boldsymbol{\varepsilon}^{tr} - \boldsymbol{\varepsilon}^{tp} \right) \tag{22}$$

$$\kappa = -\frac{\partial \phi}{\partial T} = -\nu\xi + c \ln\left(\frac{T}{T_0}\right) - \frac{1}{2}\boldsymbol{\varepsilon}^e : \frac{\partial \mathbf{C}}{\partial T} : \boldsymbol{\varepsilon}^e \tag{23}$$

From Equation (21), we get the thermodynamic driving forces for the α-th transformation system (π_{re}^{α}) and the α-th equivalent slipping system (π_{tp}^{α}):

$$\begin{aligned} \pi_{re}^{\alpha} &= g^{tr}\left(\boldsymbol{\sigma} + \mathrm{B}_{tr}\right) : \mathbf{P}^{\alpha} - \nu\left(T - T_0\right) \\ &- H^{\alpha}\xi^{\alpha} - \frac{1}{2}\boldsymbol{\varepsilon}^e : \left(\mathbf{C}_M - \mathbf{C}_A\right) : \boldsymbol{\varepsilon}^e \end{aligned} \tag{24}$$

$$\pi_{tp}^{\alpha} = \left|\boldsymbol{\sigma} : \mathbf{P}^{\alpha}\right| - H_{tp}\bar{\gamma}_{tp}^{\alpha} \tag{25}$$

The balance temperature T_0 is given as:

$$T_0 = M_f + \frac{Y_{tr}^{\alpha}}{\nu} \tag{26}$$

where M_f is the martensite finish temperature. Therefore Equation (24) is rewritten as:

$$\begin{aligned} \pi_{re}^{\alpha} &= g^{tr}\left(\boldsymbol{\sigma} + \mathrm{B}_{tr}\right) : \mathbf{P}^{\alpha} - \nu\left(T - M_f\right) \\ &H^{\alpha}\xi^{\alpha} - \frac{1}{2}\boldsymbol{\varepsilon}^e : \left(\mathbf{C}_M - \mathbf{C}_A\right) : \boldsymbol{\varepsilon}^e + Y_{tr}^{\alpha} \end{aligned} \tag{27}$$

2.3. Evolution of internal variables

Due to the thermodynamics constraints, it is supposed that the evolution of martensitic transformation keeps to a power law. Besides, the natural physical constraints of ξ and ξ^{α} must be satisfied. It is deduced that:

$$\dot{\xi}^{\alpha} = \begin{cases} \left|\dfrac{\pi_{re}^{\alpha}}{Y_{tr}^{\alpha}}\right|^{n_{tr}} sign\left(\pi_{re}^{\alpha}\right) & \text{if } 0 < \xi^{\alpha} < \xi_{sat} \text{ and } 0 < \xi < \xi_{sat} \\ 0 & \text{else} \end{cases} \tag{28}$$

where Y_{tr}^{α} is the transformation resistance and n_{tr} is the material parameter controlling the rate sensitivity of martensitic transformation. Owing to the non-viscous property of NiTi, n_{tr} should be large enough, i.e. $n_{tr} = 50$. ξ_{sat} is the saturated volume fraction of martensite and ξ_d is defined as:

$$\xi_d = 1 - \xi_{sat} \tag{29}$$

It has been experimentally observed that cyclic martensitic transformation results in the accumulation of ξ_d (Yu et al., 2014a), so ξ_d is decomposed as:

$$\xi_d = \sum_{\alpha=1}^{24} \xi_d^{\alpha} \tag{30}$$

Slipping accumulates progressively as martensitic transformation takes place, so the slipping rate of the α-th equivalent slipping system is adapted from the slipping law proposed by Berbenni et al. (2004) and Yu et al. (2014a):

$$\dot{\gamma}_{tp}^{\alpha} = \begin{cases} \gamma^{\alpha} \exp\left\{\dfrac{-\Delta G_{slip}}{k_b T}\left[1 - \left(\dfrac{\pi_{tp}^{\alpha}}{\tau_0}\right)^{p}\right]^{q}\right\} \operatorname{sign}\left(\boldsymbol{\sigma} : \mathrm{P}^{\alpha}\right)\dot{\xi}^{\alpha} \\ \qquad \text{if } \pi_{tp}^{\alpha} > 0 \\ 0 \quad \text{else} \end{cases} \tag{31}$$

where γ^{α} is the reference slipping rate of the α-th martensite variant, p ($0 < p \leq 1$) and q ($1 < q \leq 2$) are material parameters, ΔG_{slip} is the activation energy of slipping, k_b is the Boltzmann's constant, and τ_0 is the critical resolved shear stress. In order to describe superelasticity degeneration of NiTi (Kang et al., 2009; Wagner et al., 2004), γ^{α} is given by:

$$\gamma^{\alpha} = \gamma_0 \exp(-d_1 \bar{\xi}^{\alpha}) \tag{32}$$

where d_1 is the material parameter controlling the saturation rate of slipping; $\bar{\xi}^{\alpha}$ is the accumulated volume fraction of the α-th martensite variant and is defined as:

$$\dot{\bar{\xi}}^{\alpha} = \left|\dot{\xi}^{\alpha}\right| \tag{33}$$

The rate equation of dislocation density containing production and annihilation terms is formulated as (Mecking et al., 1981):

$$\dot{\rho}^{\alpha} = c_1\left(\sqrt{\rho^{\alpha}} - c_2\rho^{\alpha}\right)\left|\dot{\gamma}_{tp}^{\alpha}\right| \tag{34}$$

where c_1 and c_2 are material parameters. Equation (34) can be integrated as:

$$\sqrt{\rho^{\alpha}} = \frac{1}{c_2}\left[1 - \exp\left(-\frac{c_1 c_2}{2}\bar{\gamma}_{tp}^{\alpha}\right)\right] + \sqrt{\rho_0} \tag{35}$$

where ρ_0 is the initial dislocation density of the α-th equivalent slipping system. In order to capture the superelastic degeneration of a cyclic deformed NiTi in a more efficient way, evolution equations of B_{tr}^{α}, Y_{tr}^{α}, H^{α} and $\xi_{\mathrm{d}}^{\alpha}$ are given in explicit forms:

$$B_{\mathrm{tr}}^{\alpha} = c_3\sqrt{\rho^{\alpha}}\left[1 - \exp\left(-d_2\bar{\xi}^{\alpha}\right)\right] \tag{36}$$

$$Y_{\mathrm{tr}}^{\alpha} = Y_0 - c_4\sqrt{\rho^{\alpha}}\left[1 - \exp\left(-d_2\bar{\xi}^{\alpha}\right)\right] \tag{37}$$

$$H^{\alpha} = H_0 + c_5\sqrt{\rho^{\alpha}}\left[1 - \exp\left(-d_2\bar{\xi}^{\alpha}\right)\right] \tag{38}$$

$$\xi_{\mathrm{d}}^{\alpha} = c_6\sqrt{\rho^{\alpha}}\left[1 - \exp\left(-d_2\bar{\xi}^{\alpha}\right)\right] \tag{39}$$

where Y_0 is the initial transformation resistance, H_0 is the initial transformation hardening modulus, c_3 to c_6 are the material parameters governing the impact of dislocation

density on internal variables, and d_2 is the material parameter determining the saturation rate. It is clear that ρ^{α} acts as the numerical linkage among the variables.

For simplicity it is assumed that the elastic tensors $\mathbf{C}_A$ and $\mathbf{C}_M$ are the same and isotropic, so only elastic modulus (E) and Poisson's ratio (μ) suffice. Elastic modulus changes progressively with temperature (Yu et al., 2014a; Xiao et al., 2017), and it is proposed as:

$$E = E_{ref} + E_T(T - T_{ref}) \tag{40}$$

where E_{ref} is the elastic modulus at the reference temperature (T_{ref}) and E_T is the material parameter measuring the temperature dependence of elastic modulus.

3. Verification and discussion

3.1. Algorithm of the model

The constitutive model is implemented as VUMAT into ABAQUS/Explicit. Each element in the finite element model represents one grain. One should note that the element size is much larger than the actual grain size. Although granular constraints impose prominent impacts on the NiTi at the microstructural length-scale (Paranjape et al., 2017), it has been shown that the interaction between grains has an insignificant effect on macroscopic response (Gall et al., 2000; Long et al., 2017, 2020; Thamburaja & Anand, 2003). Therefore, the global stress-strain response is calculated from the overall reaction of the finite element model, and the proposed model can be applied to predict the behavior of a polycrystalline NiTi in an average manner. The integration algorithm of VUMAT at the (n + 1)-th step is shown in the following steps:

1. At the beginning of the (n + 1)-th step, for a given element, read the parameters of the α-th martensite variant calculated at the n-th step, i.e. $\mathbf{P}^{\alpha}$, $(\xi^{\alpha})_n$, $(\xi)_n$, $(\bar{\xi}^{\alpha})_n$, $(\xi_d^{\alpha})_n$, $(\gamma_{tp}^{\alpha})_n$, $(\bar{\gamma}_{tp}^{\alpha})_n$, $(\rho^{\alpha})_n$, $(B_{tr}^{\alpha})_n$, $(Y_{tr}^{\alpha})_n$, $(H^{\alpha})_n$ and $(\boldsymbol{\sigma})_n$, from user-defined variables. Update $(\Delta\varepsilon)_{n+1}$ provided by Abaqus.
2. Calculate π_{re}^{α} and $\Delta\xi^{\alpha}$.
3. In order to maintain the martensite volume fraction within the rational range and avoid numerical divergence, $\Delta\xi^{\alpha}$ obtained at step (2) will be adjusted according to:
   – If $\Delta\xi^{\alpha} > 0$ and
   $\Delta\xi^{\alpha} > \min(\xi_{sat} - (\xi^{\alpha})_n; \xi_{sat} - (\xi)_n)$,
   $\Delta\xi^{\alpha} = \min(\xi_{sat} - (\xi^{\alpha})_n; \xi_{sat} - (\xi)_n)$
   – If $\Delta\xi^{\alpha} < 0$ and $\Delta\xi^{\alpha} < -(\xi^{\alpha})_n$, $\Delta\xi^{\alpha} = -(\xi^{\alpha})_n$
   where $\min(a;b) = \begin{cases} a & \text{if } a < b \\ b & \text{if } a \geq b \end{cases}$
4. Update $(\xi^{\alpha})_{n+1}$, $(\xi)_{n+1}$, $(\bar{\xi}^{\alpha})_{n+1}$, $(\xi_d^{\alpha})_{n+1}$, $(\gamma_{tp}^{\alpha})_{n+1}$, $(\bar{\gamma}_{tp}^{\alpha})_{n+1}$, $(\rho^{\alpha})_{n+1}$, $(B_{tr}^{\alpha})_{n+1}$, $(Y_{tr}^{\alpha})_{n+1}$, $(H^{\alpha})_{n+1}$ and $(\boldsymbol{\sigma})_{n+1}$. Write them into user defined variables.
5. Traverse all the elements and α (α = 1, 2, ..., 24). End the program and start the next step.

3.2. Numerical tests

In this paper, we focus on the quasi-static behavior of a thin-walled cylinder NiTi tube. It is reported that the NiTi tube exhibits dominant <111> texture along the drawing direction (Gall et al., 2000; Long et al., 2017, 2020; Otsuka & Ren, 2005; Thmaburaja & Anand, 2003; Xiao et al., 2018; Yu et al., 2014a, 2014b, 2015, 2017). In VUMAT, the crystals are assigned as <111>, <1$\bar{1}$0> and <11$\bar{2}$> directions in a longitudinal direction and two transverse directions with a random fluctuation within the range of 5° (Gall et al., 2000; Long et al., 2017). The axial strain ε_a and the axial stress σ_a are defined as:

$$\varepsilon_a = \frac{\Delta L}{L}, \quad \sigma_a = \frac{4F}{\pi\left(D^2 - d^2\right)} \tag{41}$$

where ΔL is the axial deformation, L is the gauge length, d is the inner diameter, D is the outer diameter, and F is the applied axial force. In accordance to the experimental work (Yu et al., 2014a), the inner diameter, outer diameter and a gauge length of the numerical model are 2.3 mm, 2.5 mm and 15 mm, respectively. The model is meshed with 2400 ABAQUS-C3D8R elements to eliminate mesh sensitivity (see Appendix Fig. A1). Both the experimental sample and the numerical model are cycled between 10% axial strain and axial-stress-free state. Material parameters of the constitutive model are listed in Table 2.

Figures 1 to 3 show the representative stress-strain curves of NiTi at 313K, 333K and 353K. The evolutions of residual strain and dissipation energy are illustrated in Figure 4. It can be seen clearly that the deterioration features of a superelastic NiTi, i.e. the accumulation of retained strain, the increasing transformation hardening, the drop and shrinkage of transformation plateau, and the reduction of dissipation energy, are fully reproduced (Kang et al., 2009; Song et al., 2015; Wagner et al., 2004; Yu et al., 2014a). The mechanical response gets stabilized and the mechanical parameters get saturated after certain cycles. In general, the simulated responses match well with the experimental data (Yu et al., 2014a).

Table 2. Material parameters of the numerical model

$p = 0.05$	$q = 1.0$	$\Delta G_{slip} = 4.4 \times 10^{-19}$ N/m
$k_b = 1.38 \times 10^{-23}$ J/K	$\tau_0 = 300$ MPa	$\gamma_0 = 1.7 \times 10^{-2}$
$\rho_0 = 1 \times 10^{14}$ /m^2	$H_{tp} = 500$ MPa	$H_0 = 10$ MPa
$Y_0 = 10$ MPa	$g^{tr} = 0.165$	$v = 0.365$ MPa/K
$M_f = 208$ K	$n_{tr} = 50$	$c_1 = 1 \times 10^{10}$ /m
$c_2 = 1 \times 10^{-8}$ m	$c_3 = 1 \times 10^{-6}$ N/m	$c_4 = 9 \times 10^{-8}$ N/m
$c_5 = 3 \times 10^{-7}$ N/m	$c_6 = 9 \times 10^{-10}$ m	$d_1 = 0.65$
$d_2 = 0.8$	$E_{ref} = 22$ GPa	$T_{ref} = 313$ K
$E_T = 0.225$ GPa/K	$\mu = 0.3$	

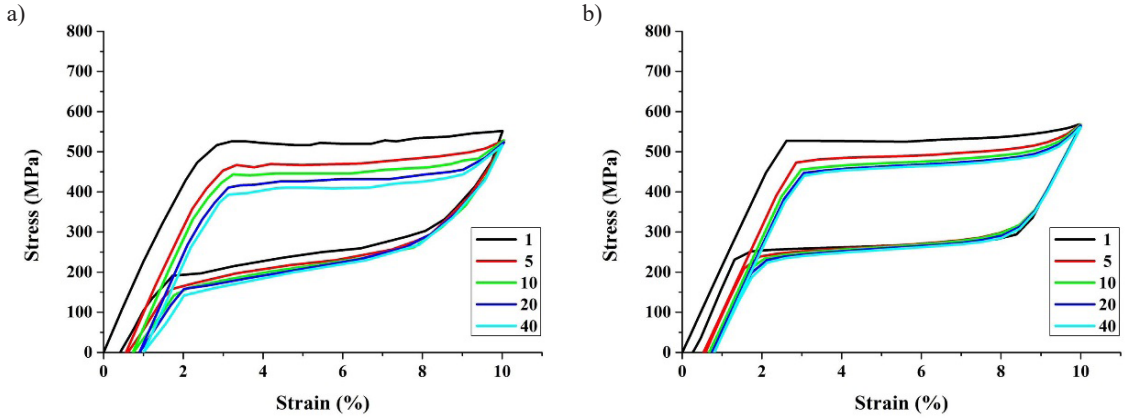

Fig. 1. Stress-strain curves of NiTi tube subjected to uniaxial tension at 313 K at the 1st, 5th, 10th, 20th and 40th cycles: a) experimental data (Yu et al., 2014a); b) simulation results

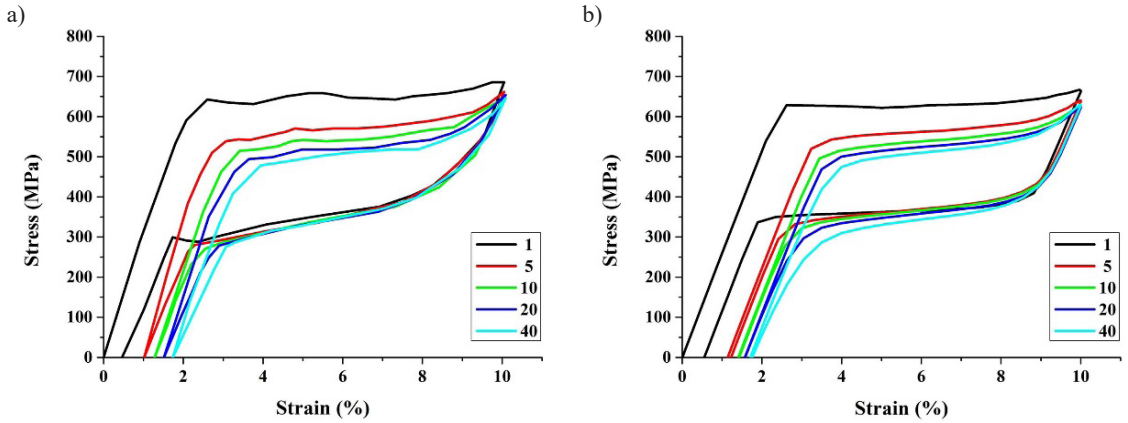

Fig. 2. Stress-strain curves of NiTi tube subjected to uniaxial tension at 333 K at the 1st, 5th, 10th, 20th and 40th cycles: a) experimental data (Yu et al., 2014a); b) simulation results

Figures 1 to 4 also manifest that the increment of temperature facilitates superelastic degradation of NiTi. This phenomenon can be attributed to the following reasons. On the one hand, as demonstrated in Equation (31), the temperature is positively related to slipping rate. On the other hand, due to the inherent Clausius–Clapeyron relation of the NiTi (Churchill et al., 2009; Liu et al., 2008; Xiao et al., 2017), the driving force for slipping (π_{tp}^{α}) is larger at higher temperatures and gives rise to a higher slipping rate. It is evident that a higher slipping rate will lead to more intense dislocation generation. Since all the internal variables are intrinsically linked to dislocation density, more severe superelastic degeneration will take place at higher temperatures.

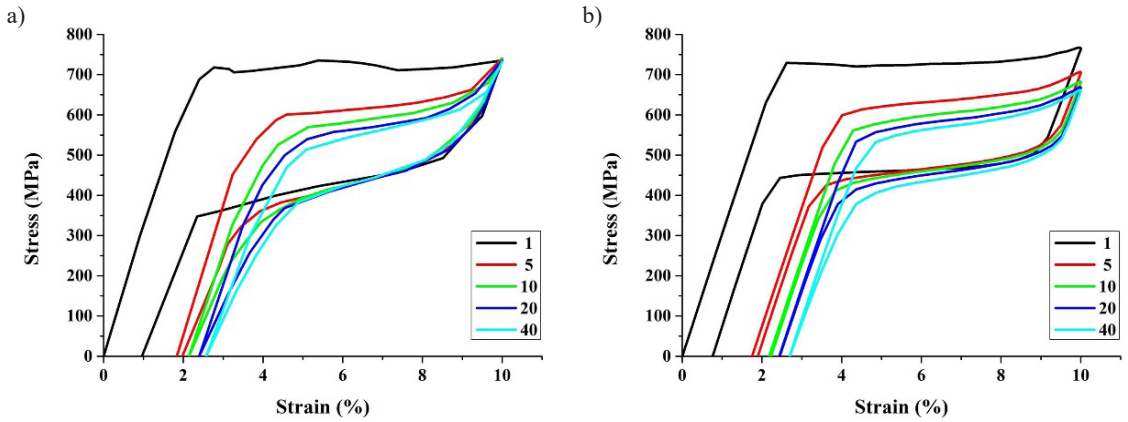

Fig. 3. Stress-strain curves of NiTi tube subjected to uniaxial tension at 353 K at the 1st, 5th, 10th, 20th and 40th cycles: a) experimental data (Yu et al., 2014a); b) simulation results

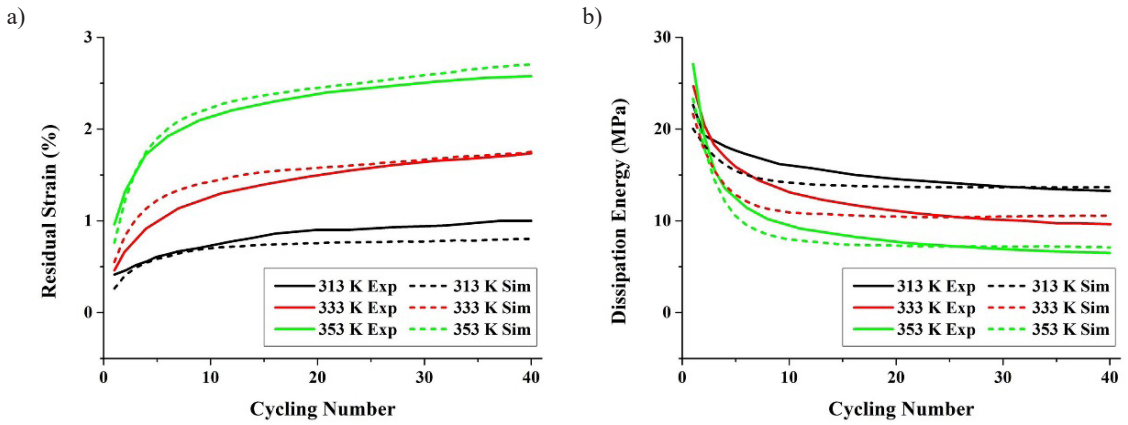

Fig. 4. Evolution curves of residual strain (a) and dissipation energy (b). Solid lines and dashed lines denote experimental data (Yu et al., 2014a) and simulation results, respectively

To demonstrate the predictive capability of the proposed model, two series of mechanical responses of superelastic NiTi tubes subjected to 20 cyclic bending at 313 K and 353 K were furnished. In order to highlight the inhomogeneous deformation upon bending, the inner diameter (d), outer diameter (D) and gauge length (L) of the numerical model were set as 1.25 mm, 2.5 mm and 15 mm, respectively. As can be seen in Figure 5, bending loads are applied at both ends of the tube, compelling bending moment (M_x)/rotation degree (θ_x) cycles between M_x = 0 Nm and θ_x = 0.6 rad. Due to the symmetry of the mid-span (x-y plane), only half of the model is under consideration and the results are mirrored about the mid-span.

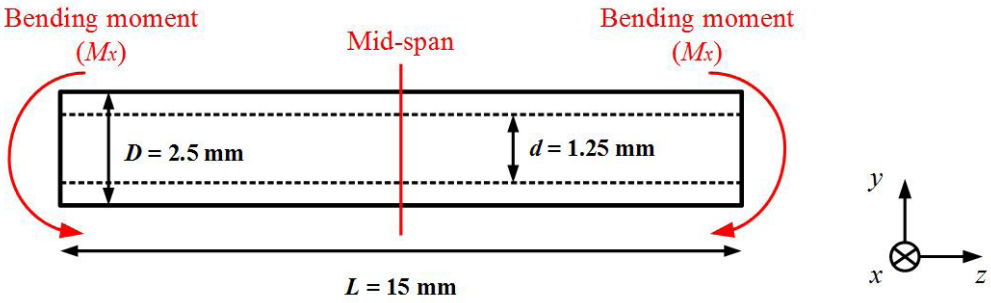

Fig. 5. Schematic illustration of the bending model. Specimen coordinates are shown at lower right

Representative moment (M_x)-rotation (θ_x) curves are shown in Figure 6. As expected, the residual deformation accumulates more drastically at 353 K than at 313 K. Figures 7 and 8 depict the contour plots of longitudinal logarithmic strain (denoted as LE33) at moment-free state and the peak loading at the 1st, 5th, 10th and 20th cycles. Clearly, the introduction of the texture leads to tension-compression asymmetry of the NiTi tube and the difference in longitudinal strain between the tensile side and compressive side is witnessed. This phenomenon is also experimentally verified by means of digital image correlation (Bechle & Kyriakides, 2014, 2016; Reedlunn et al., 2014, 2020). The residual strain concentrates mainly on the tensile side while the strain distribution is essentially identical at the peak loading regardless of temperature variation.

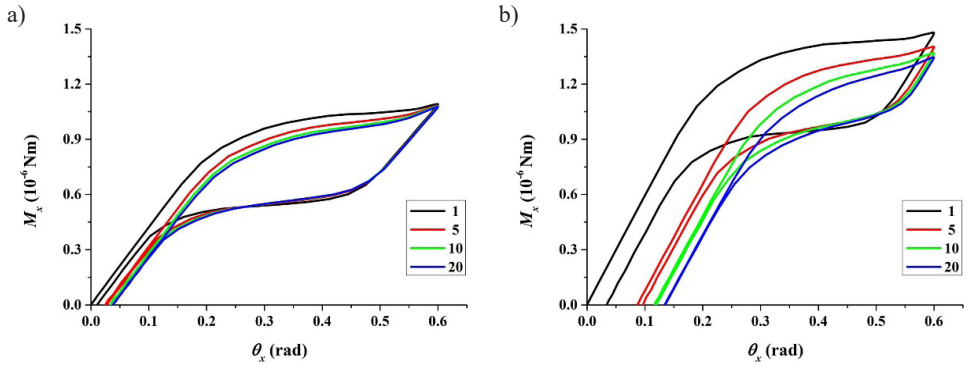

Fig. 6. Predicted moment (M_x)-rotation (θ_x) curves of NiTi tube subjected to cyclic bending at the 1st, 5th, 10th and 20th cycles at 313 K (a) and at 353 K (b)

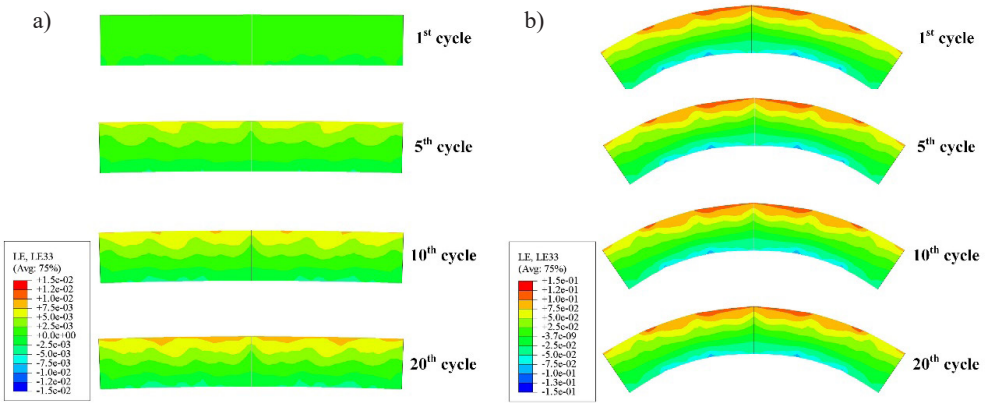

Fig. 7. Longitudinal strain distribution and deformation profile of the NiTi tube subjected to cyclic bending at 313 K at the 1st, 5th, 10th and 20th cycles at moment-free state (a) and at the peak loading (b)

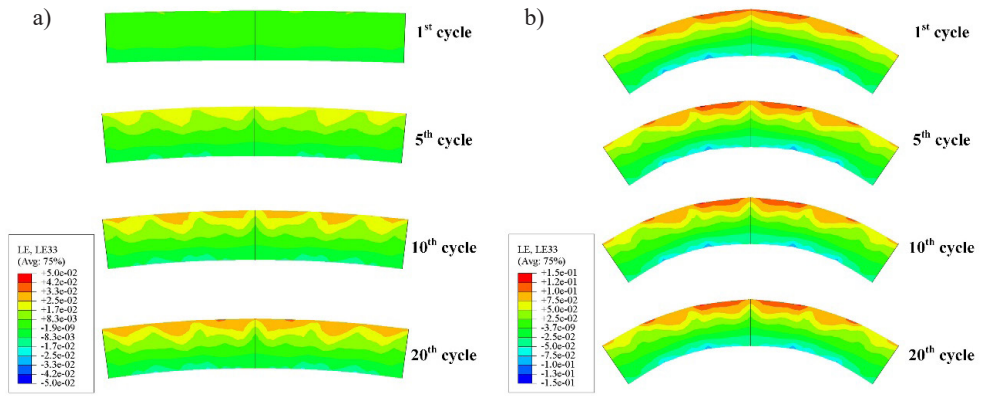

Fig. 8. Longitudinal strain distribution and deformation profile of the NiTi tube subjected to cyclic bending at 353 K at 1st, 5th, 10th and 20th cycles at moment-free state (a) and at the peak loading (b)

4. Conclusions

The present paper has developed a robust three-dimensional micromechanical-based constitutive model for a cyclic deformed superelastic NiTi. The dominant texture of the NiTi tube is prescribed as <111> direction along the longitudinal direction. Through implementation into finite element software, the constitutive model is extended from the single-crystal scale to a polycrystalline version and the global stress-strain response is obtained from the overall reaction of the model.

Several numerical tests were performed to show the reliability and predicting the capacity of the model. By taking several physical mechanisms into account, the accumulation of transformation-induced plasticity, the increase of back stress, the decrease of stress hysteresis, and the drop of saturated martensite volume fraction are introduced into the model. It has been verified that the superelastic degeneration of a NiTi has been reasonably reproduced. Through linking the internal variables to dislocation density, the temperature dependence of a cyclic deformed superelastic NiTi has also been soundly duplicated. Furthermore, two practical examples demonstrating the mechanical behavior of a superelastic NiTi tube subjected to cyclic bending have been furnished.

Acknowledgements

Yao Xiao acknowledges the financial support of the Shanghai Sailing Program (Grant No. 22YF1450600) and the Fundamental Research Funds for the Central Universities. Jianping Lin appreciates the support of the Natural National Science Foundation of China (Grant No. 52075390).

Appendix

Mesh sensitivity is checked in the sample deformed at 353 K. The model is meshed with 1600 elements (coarsen mesh), 2400 elements (original mesh) and 3240 elements (refined mesh) as seen in Figure A1. The simulation results are essentially identical, indicating the mesh dependence are excluded. The model with 2400 elements was used in the present work for the sake of accuracy and efficiency.

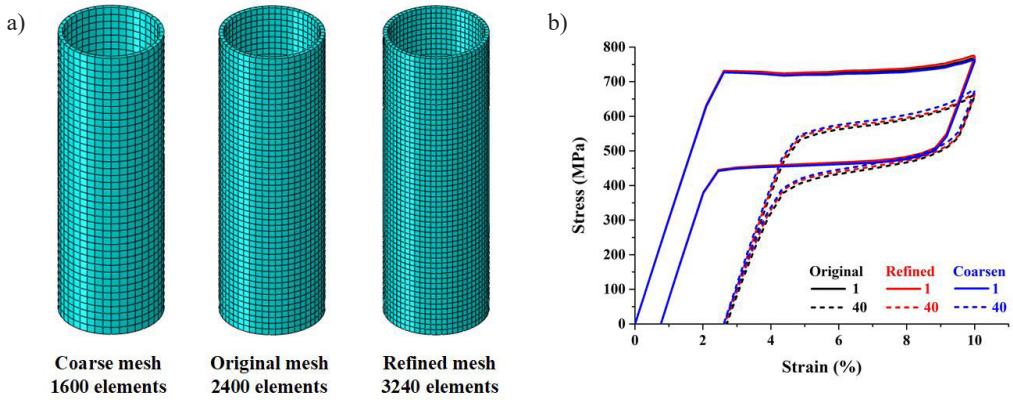

Fig. A1. Numerical model (a) and simulation results (b) of the sample deformed at 353 K at the 1st cycle and 40th cycles

References

Bechle, N.J., & Kyriakides, S. (2014). Localization in NiTi tubes under bending. *International Journal of Solids Structures*, *51*(5), 967–980.

Bechle, N.J., & Kyriakides, S. (2016). Evolution of localization in pseudoelastic NiTi tubes under biaxial stress states. *International Journal of Plasticity*, *82*, 1–31.

Berbenni, S., Favier, V., Lemoine, X., & Berveiller, M. (2004). Micromechanical modeling of the elastic-viscoplastic behavior of polycrystalline steels having different microstructures. *Materials Science and Engineering A*, *372*(1–2), 128–136.

Churchill, C.B., Shaw, J.A., & Iadicola, M.A. (2009). Tips and tricks for characterizing shape memory alloy wire: part 2 – fundamental isothermal responses. *Experimental Techniques*, *33*(1), 51–62.

Cisse, C., Zaki, W., & Zineb, T.B. (2016). A review of constitutive models and modeling techniques for shape memory alloys. *International Journal of Plasticity*, *76*, 244–284.

Dhala, S., Mishra, S., Tewari, A., & Alankar, A. (2019). Modeling of finite deformation of pseudoelastic NiTi shape memory alloy considering various inelasticity mechanisms. *International Journal of Plasticity*, *115*, 216–237.

Gall, K., Lim, T.J., McDowell, D.L., Sehitoglu, H., & Chumlyakov, Y.I. (2000). The role of intergranular constraint on the stress-induced martensitic transformation in textured polycrystalline NiTi. *International Journal of Plasticity*, *16*(10–11), 1189–1214.

Kang, G., Kan, Q., Qian, L., & Liu, Y. (2009). Ratchetting deformation of super-elastic and shape-memory NiTi alloys. *Mechanics of Materials*, *41*(2), 139–153.

Liu, Y., Mahmud, A., Kursawe, F., & Nam, T.H. (2008). Effect of pseudoelastic cycling on the Clausius–Clapeyron relation for stress-induced martensitic transformation in NiTi. *Journal of Alloys and Compounds*, *449*(1–2), 82–87.

Long, X., Peng, X., Fu, T., Tang, S., & Hu, N. (2017). A micro-macro description for pseudoelasticity of NiTi SMAs subjected to nonproportional deformations. *International Journal of Plasticity*, *90*, 44–65.

Long, X., Peng, X., & Fu, T. (2020). Extension of micromechanics model and micro-macro description to shape memory effect of NiTi SMAs. *International Journal of Solids Structures*, *188–189*, 169–180.

Manchiraju, S., & Anderson, P.M. (2010). Coupling between martensitic phase transformations and plasticity: A microstructure-based finite element model. *International Journal of Plasticity*, *26*(10), 1508–1526.

Mecking, H., & Kocks, U.F. (1981). Kinetics of flow and strain-hardening. *Acta Metallurgica*, *29*(11), 1865–1875.

Otsuka, K., & Ren, X. (2005). Physical metallurgy of Ti–Ni-based shape memory alloys. *Progress in Materials Science*, *50*(5), 511–678.

Paranjape, H.M., Paul, P.P., Sharma, H., Kenesei, P., Park, J.S., Duerig, T.W., Brinson, L.C., & Stebner, A.P. (2017). Influences of granular constraints and surface effects on the heterogeneity of elastic, superelastic, and plastic responses of polycrystalline shape memory alloys. *Journal of the Mechanics and Physics of Solids*, *102*, 46–66.

Reedlunn, B., Churchill, C.B., Nelson, E.E., Shaw, J.A., & Daly, S.H. (2014). Tension, compression, and bending of superelastic shape memory alloy tubes. *Journal of the Mechanics and Physics of Solids*, *63*, 506–537.

Reedlunn, B., LePage, W.S., Daly, S.H., & Shaw, J.A. (2020). Axial-torsion behavior of superelastic tubes: Part I, proportional isothermal experiments. *International Journal of Solids Structures*, 199, 1–35.

Sadjadpour, A., & Bhattacharya, K. (2007). A micromechanics-inspired constitutive model for shape-memory alloys. *Smart Materials and Structures*, *16*(5), 1751–1765.

Šittner, P., Sedlák, P., Seiner, H., Sedmák, P., Pilch, J., Delville, R., Heller, L., & Kadeřávek, L. (2018). On the coupling between martensitic transformation and plasticity in NiTi: Experiments and continuum based modelling. *Progress in Materials Science*, *98*, 249–298.

Song, D., Kang, G., Kan, Q., Yu, C., & Zhang, C. (2015). Damage-based life prediction model for uniaxial low-cycle stress fatigue of super-elastic NiTi shape memory alloy microtubes. *Smart Materials and Structures*, *24*(8), 085007.

Thamburaja, P., & Anand, L. (2003). Thermo-mechanically coupled superelastic response of initially-textured Ti–Ni sheet. *Acta Materialia*, *51*(2), 325–338.

Wagner, M., Sawaguchi, T., Kausträter, G., Höffken, D., & Eggeler, G. (2004). Structural fatigue of pseudoelastic NiTi shape memory wires. *Materials Science and Engineering A*, *378*(1–2), 105–109.

Wang, X.M., Xu, B.X., & Yue, Z.F. (2008). Micromechanical modelling of the effect of plastic deformation on the mechanical behaviour in pseudoelastic shape memory alloys. *International Journal of Plasticity*, *24*(8), 1307–1332.

Xiao, Y., & Jiang, D. (2020). Constitutive modelling of transformation pattern in superelastic NiTi shape memory alloy under cyclic loading. *International Journal of Mechanical Science*, *182*, 105743.

Xiao, Y., Zeng, P., Lei, L., & Zhang, Y. (2017). In situ observation on temperature dependence of martensitic transformation and plastic deformation in superelastic NiTi shape memory alloy. *Materials & Design*, *134*, 111–120.

Xiao, Y., Zeng, P., & Lei, L. (2018). Micromechanical modeling on thermomechanical coupling of cyclically deformed superelastic NiTi shape memory alloy. *International Journal of Plasticity*, *107*, 164–188.

Yan, B., Jiang, S., Hu, L., Zhang, Y., & Sun, D. (2021). Crystal plasticity finite element simulation of NiTi shape memory alloy under canning compression based on constitutive model containing dislocation density. *Mechanics of Materials*, *157*, 103830.

Yu, C., Kang, G., & Kan, Q. (2014a). A physical mechanism based constitutive model for temperature-dependent transformation ratchetting of NiTi shape memory alloy: One-dimensional model. *Mechanics of Materials*, *78*, 1–10.

Yu, C., Kang, G., & Kan, Q. (2014b). Crystal plasticity based constitutive model of NiTi shape memory alloy considering different mechanisms of inelastic deformation. *International Journal of Plasticity*, *54*, 132–162.

Yu, C., Kang, G., Song, D., & Kan, Q. (2015). Effect of martensite reorientation and reorientation-induced plasticity on multiaxial transformation ratchetting of super-elastic NiTi shape memory alloy: New consideration in constitutive model. *International Journal of Plasticity*, *67*, 69–101.

Yu, C., Kang, G., Kan, Q., & Xu, X. (2017). Physical mechanism based crystal plasticity model of NiTi shape memory alloys addressing the thermo-mechanical cyclic degeneration of shape memory effect. *Mechanics of Materials*, *112*, 1–17.